https://doi.org/10.5194/angeo-2019-154
Preprint. Discussion started: 25 November 2019

Annales Geophysicae Discussions

Nighttime $O(^1D)$ distributions in the mesopause region derived from SABER data

Mikhail Yu. Kulikov[1], and Mikhail V. Belikovich[1]
[1]Institute of Applied Physics of the Russian Academy of Sciences, 46 Ulyanov Str., 603950 Nizhny Novgorod, Russia
Correspondence to: Mikhail Yu. Kulikov (mikhail_kulikov@mail.ru)

Abstract. In this study, the new source of $O(^1D)$ in the mesopause region proposed by Kalogerakis (2019) is applied to SABER data to estimate the nighttime $O(^1D)$ distributions for the years 2003-2005. It is found that $O(^1D)$ evolutions in these years are very similar to each other. Depending on the month, monthly averaged $O(^1D)$ distributions may have a pronounced maximum (up to 80-110 cm^{-3} in January and July) localized in height (at ~97±4 km) and latitude (at ~52±4°S or ~52±4°N). The nightly averaged $O(^1D)$ concentrations may reach ~300 cm^{-3}. The obtained results are useful data set for subsequent estimation of nighttime $O(^1D)$ influence on chemistry of the mesopause region.

1 Introduction

Daytime $O(^1D)$ is considered to be one of the important chemical minor species of the stratosphere, mesosphere and thermosphere, as it plays a significant role in the chemistry, and the radiative and thermal balance of this region (Brasseur & Solomon, 2005). First of all, formed by photolysis of O_2 and O_3, $O(^1D)$ is a mediator involved in the transformation of absorbed solar radiation energy into the heating of this region and, in particular, excitation of $N_2(v)$ and $CO_2(v)$ (Harris & Adams, 1983; Panka et al., 2017). Also, $O(^1D)$ atoms participate in the reactions of destruction of long-lived greenhouse gases (Baasandorj et al., 2012), CH_4 oxidation, and HO_x and NO_x production, for example:

$O(^1D)+N_2O \rightarrow 2NO$

$O(^1D)+H_2O \rightarrow 2OH$

$O(^1D)+H_2 \rightarrow H+OH$

$O(^1D)+CH_4 \rightarrow CH_3+OH$

$O(^1D)+CH_4 \rightarrow H_2+CH_2O$

Moreover, the red line emission from $O(^1D)$ atoms is one of the most important airglow phenomenon which are used as a diagnostic of the ionosphere, for example, to monitor the electron density and neutral winds in the F region (Shepherd et al., 2019). Therefore, many papers and experimental campaigns are devoted to measurements of features of O_3 photolysis to $O(^1D)$ (Taniguchi et al., 2003; Hofzumahaus et al., 2004).

Until recently, it was believed that the above mentioned processes stopped at night due to absent of constant source of $O(^1D)$ in this time and extremely low (less than 1 s) life time of this component. In principle, $O(^1D)$ can be generated in sprite halos but for a low duration of 1 ms (Hiraki et al., 2004). In this year, based on laboratory experiments, Kalogerakis (2019) highlighted a previously unrecognized source of nighttime $O(^1D)$ and O_2 A-band emission in the mesopause region via process:

$$OH(v \geq 5) + O(^3P) \rightarrow OH(0 \leq v' \leq v-5) + O(^1D), \quad (1)$$

that is multiquantum quenching of high excited states of OH by collisions with atomic oxygen in ground state. Taking into account the major way of this process (Kalogerakis et al., 2016):

$$OH(9) + O(^3P) \rightarrow OH(3) + O(^1D), \quad (2)$$

Kalogerakis (2019) showed that a new model of O_2 A-band well described (qualitatively and quantitatively) the results of early nighttime rocket measurements of volume emission rate profiles of this airglow. Thus, he proved that the process (1) really took place in mesopause region and the way (2) was the major source of $O(^1D)$.

https://doi.org/10.5194/angeo-2019-154
Preprint. Discussion started: 25 November 2019

In this study, the new source of $O(^1D)$ in the mesopause region proposed by Kalogerakis (2019) is applied to SABER data to estimate the $O(^1D)$ nighttime distributions for the years 2003-2005.

2 $O(^1D)$ model and method of derivation from SABER Data

Following Kalogerakis (2019), the nighttime balance of OH(9) and $O(^1D)$ concentrations in the mesopause region is determined by processes summarized in Table 1. Due to low values of chemical lifetimes (less than 1 s), these components can be considered in chemical equilibrium:

$$OH(9) = \frac{y_9 \cdot k_1 \cdot H \cdot O_3}{k_2 \cdot O_2 + k_3 \cdot N_2 + k_4 \cdot O + k_5}, \quad (3)$$

$$O(^1D) = \frac{y_1 \cdot k_4 \cdot OH(9) \cdot O}{k_6 \cdot O_2 + k_7 \cdot N_2 + k_8} = \frac{y_1 \cdot y_9 \cdot k_1 \cdot k_4 \cdot O \cdot H \cdot O_3}{(k_2 \cdot O_2 + k_3 \cdot N_2 + k_4 \cdot O + k_5) \cdot (k_6 \cdot O_2 + k_7 \cdot N_2 + k_8)}, \quad (4)$$

where k_i are the corresponding process rate coefficients. Thus, local $O(^1D)$ concentration is defined by the values of temperature (T), and concentrations of M, O_3, O, and H. We suggest getting this information from satellite-based observations.

Mlynczak et al. (2013, 2014) proposed the method of nighttime O and H derivation in the range of 0.01–0.0001 hPa (approximately 80–105 km) from simultaneous measurements of temperature, ozone (using ozone emission at 9.6 μm) and OH(9–7) and OH(8–6) band emissions by the SABER (Sounding of the Atmosphere using Broadband Emission Radiometry) instrument onboard the TIMED (Thermosphere Ionosphere Mesosphere Energetics and Dynamics) satellite. The method used two assumptions: the chemical equilibrium condition for nighttime ozone, and the model of OH(9–7) and OH(8–6) emissions. Recently (Mlynczak et al. (2018), the parameters of the model was corrected. So now, O distributions derived from SABER data are in good consistent with O distributions obtained from SCIAMACHY green-line and OH nightglow measurements (Zhu & Kaufmann, 2019). In this work, we derive the local values of O and H from SABER data and apply all sets of data (T, concentrations of M, O_3, O, and H) to retrieve the local concentrations of $O(^1D)$ with the use of eq. (4). At this, we use also the analytical criterion (Kulikov et al., 2018) that allows the localization of the lower boundary of nighttime ozone chemical equilibrium (Kulikov et al., 2019) with the use of SABER data.

3 $O(^1D)$ nighttime distributions

We use the version 2.0 of the SABER data product (Level2A) for the simultaneously measured O_3, volume emission rate of OH from the v = 9 and v = 8 states and temperature profiles within the 0.01–0.0001 hPa pressure (p) interval (approximately 80–105 km in 2003-2005. We take only nighttime data when the solar zenith angle $\chi > 95°$. Appling the mentioned criterion for each set of simultaneously measured profiles, we find the local position (the pressure level p_{eq}) of the boundary of nighttime ozone chemical equilibrium. Thus, we take into account only the upper part of each SABER profile corresponding $p \geq p_{eq}$. The range of latitudes covered by the satellite trajectory in a month was divided into 20 bins ~ $(5\text{-}8)^{\circ}$ each. 1500-3000 single profiles of $O(^1D)$ concentration fall into one bin during a month of SABER observations (or 50-100 profiles per a one night). For each bin we calculate monthly and nightly averaged zonal mean $< O(^1D) >$distributions (hereafter, the angle brackets are used to denote timely and spatially averaged values).

Monthly averaged $< O(^1D) >$ distributions in corresponding month of 2003-2005 are shown in Figs. 1–3. Firstly, it can be noted that $O(^1D)$ evolutions in these years are very similar to each other. Secondly, many features of $O(^1D)$ in the southern hemisphere are repeated in the northern hemisphere with a shift of 6 months. In particular, $O(^1D)$ concentration distributions in January-February and November-December have a pronounced maximum (up to 80 cm^{-3} in January) localized in height (at ~97±4 km) and latitude (at ~52±4°S). In May-August, the distributions have similar maximum (up to 110 cm^{-3} in July) localized at ~98±3 km and ~52±4°N. In other months (March-April and September-November), one can see transitional $O(^1D)$ distributions with several maxima but their values don't exceed (30-35) cm^{-3}. Figs. 4–5 show the nightly averaged

https://doi.org/10.5194/angeo-2019-154
Preprint. Discussion started: 25 November 2019

$< O(^1D) >$ vertical distributions at (48-54)°N and (48-54)°S as a function of day of year. Examples of these profiles are presented in Fig. 6. One can see that local value of $< O(^1D) >$ at ~(97-98) km may reach ~300 cm^{-3} in both hemispheres. The uncertainty of local $O(^1D)$ concentration is defined mainly by local uncertainty of O derivation. Taking into account the O uncertainty profile presented in Mlynczak et al. (2013), we estimate that uncertainty of local $O(^1D)$ varies in the range of (30-40)% depending on the pressure level. Due to averaging, the uncertainty of nightly averaged $O(^1D)$ shown in Fig. 6 is estimated to be less than 6%.

4 Discussion and Conclusion

According to different early papers (Nicolet, 1959; Ghosh & Gupta, 1970; Shimazaki & Laird, 1970; Harris & Adams, 1983), daytime $O(^1D)$ concentrations at 90-100 km varied in the range of (10^2-10^4) cm^{-3}. Brasseur & Solomon (2005) published the table (see Table A.6.2.c) where daytime $O(^1D)$ changed from 70 cm^{-3} at 90 km to 140 cm^{-3} at 100 km. The presented results show that monthly and nightly mean nighttime $O(^1D)$ concentrations at these altitudes can reach 100 cm^{-3} and 300 cm^{-3}, respectively. Thus, nighttime concentrations of $O(^1D)$ are comparable with daytime concentrations of this component and, in principle, can impact noticeably the chemistry and thermal balance of the mesopause region. More detailed analyze of this impact should be carried out with the use of the global 3D chemical transport model of the mesosphere – lower thermosphere.

Data availability. The SABER data used in this study can be downloaded from ftp://saber.gats-inc.com/Version2_0/Level2A/. The presented data can be downloaded from http://www.iapras.ru/english/structure/dep_240/dep_240.html.

Author contributions. Both authors contributed equally to this paper.

Competing interests. The authors declare that they have no conflict of interest.

Acknowledgments. The authors are grateful the SABER team for data availability.

References

Baasandorj, M., Hall, B. D., and Burkholder, J. B.: Rate coefficients for the reaction of $O(^1D)$ with the atmospherically long-lived greenhouse gases NF_3, SF_5CF_3, CHF_3, C_2F_6, c-C_4F_8, n-C_5F_{12}, and n-C_6F_{14}. Atmos. Chem. Phys., 12, 11753-11764, doi:10.5194/acp-12-11753-201, 2012.

Brasseur, G. P., and Solomon, S.: Aeronomy of the middle atmosphere: Chemistry and physics of the stratosphere and mesosphere (3rd ed). Dordrecht, Netherlands: Springer Science and Business Media, 2005.

Burkholder, J. B., Sander, S. P., Abbatt, J., Barker, J. R., Huie, R. E., Kolb, C. E., et al.: Chemical kinetics and photochemical data for use in atmospheric studies, evaluation no. 18, JPL Publication 15–10, Pasadena, CA: Jet Propulsion Laboratory, http://jpldataeval.jpl.nasa.gov, 2015.

Ghosh, S. N., and Gupta, S. K.: Altitude distributions of and radiations from certain oxygen and nitrogen metastable constituents, J. Geomagn. Geoelectr., 22, 329-339, 1970.

Harris, R. D., and Adams, G. W.: Where does the $O(^1D)$ energy go? J. Geophys. Res., 88(A6), 4918–4928, doi:10.1029/JA088iA06p04918, 1983.

https://doi.org/10.5194/angeo-2019-154
Preprint. Discussion started: 25 November 2019

Hiraki, Y., Tong, L., Fukunishi, H., Nanbu, K., Kasai, Y., and Ichimura, A.: Generation of metastable oxygen atom $O(^1D)$ in sprite halos, Geophys. Res. Lett., 31, L14105, doi:10.1029/2004GL020048, 2004.

Hofzumahaus, A., Lefer, B. L., Monks, P. S., Hall, S. R., Kylling, A., Mayer B. et al.: Photolysis frequency of O_3 to $O(^1D)$: Measurements and modeling during the International Photolysis Frequency Measurement and Modeling Intercomparison (IPMMI), J. Geophys. Res., 109, D08S90, doi:10.1029/2003JD004333, 2004.

Hunt, B. G.: A diffusive-photochemical study of the mesosphere and lower thermosphere and the associated conservation mechanisms, J. Atm. Terr. Phys., 33, 1869-1892, 1971.

Kalogerakis, K. S., Smith, G. P., and Copeland, R. A.: Collisional removal of OH(X $^2\Pi$, v = 9) by O, O_2, O_3, N_2, and CO_2. J. Geophys. Res., 116, D20307, doi:10.1029/2011JD015734, 2011.

Kalogerakis, K. S., Matsiev, D., Sharma, R. D., and Wintersteiner, P. P.: Resolving the mesospheric nighttime 4.3 µm emission puzzle: Laboratory demonstration of new mechanism for OH(υ) relaxation, Geophys. Res. Lett., 43, 8835–8843, doi:10.1002/2016GL069645, 2016.

Kalogerakis, K. S.: A previously unrecognized source of the O2 atmospheric band emission in earth's nightglow. Science Advances, 5, eaau9255, doi:10.1126/sciadv.aau9255, 2019.

Kulikov, M. Y., Belikovich, M. V., Grygalashvyly, M., Sonnemann, G. R., Ermakova, T. S., Nechaev, A. A., and Feigin, A. M.: Nighttime ozone chemical equilibrium in the mesopause region, J. Geophys. Res., 123, 3228–3242, doi:10.1002/2017JD026717, 2018.

Kulikov, M. Yu., Nechaev, A. A., Belikovich, M. V., Vorobeva, E. V., Grygalashvyly, M., Sonnemann, G. R., and Feigin, A. M.; Border of nighttime ozone chemical equilibrium in the mesopause region from saber data: implications for derivation of atomic oxygen and atomic hydrogen, Geophys. Res. Lett., 46, 997–1004, doi:10.1029/2018GL080364, 2019.

Mlynczak, M. G., Hunt, L. A., Mast, J. C., Marshall, B. T., Russell III, J. M., Smith, A. K., Siskind, D. E., Yee, J.-H., Mertens, C. J., Martin-Torres, F. J., Thompson, R. E., Drob, D. P., and Gordley, L. L.: Atomic oxygen in the mesosphere and lower thermosphere derived from SABER: Algorithm theoretical basis and measurement uncertainty, J. Geophys. Res., 118, 5724–5735, doi:10.1002/jgrd.50401, 2013.

Mlynczak, M. G., Hunt, L. A., Marshall, B. T., Mertens, C. J., Marsh, D. R., Smith, A. K., Russell, J. M., Siskind, D. E., and Gordley, L. L.: Atomic hydrogen in the mesopause region derived from SABER: Algorithm theoretical basis, measurement uncertainty, and results, J. Geophys. Res., 119, 3516–3526, doi:10.1002/2013JD021263, 2014.

Mlynczak, M. G., Hunt, L. A., Russell, J. M., III, and Marshall, B. T.: Updated SABER night atomic oxygen and implications for SABER ozone and atomic hydrogen, Geophys. Res. Lett., 45, 5735–5741, doi:10.1029/2018GL077377, 2018.

Nicolet, M.: The constitution and composition of the upper atmosphere, Proc. IRE, 47, 142-147, 1959.

Panka, P. A., Kutepov, A. A., Kalogerakis, K. S., Janches, D., Russell, J. M., Rezac, L., Feofilov, A. G., Mlynczak, M. G., and Yiğit, E.: Resolving the mesospheric nighttime 4.3 µm emission puzzle: Comparison of the CO2(ν_3) and OH(ν) emission models, Atm. Chem. Phys., 17, 9751–9760, doi:10.5194/acp-17-9751-2017, 2017.

Sharma, R. D., Wintersteiner, P. P., and Kalogerakis, K. S.: A new mechanism for OH vibrational relaxation leading to enhanced CO_2 emissions in the nocturnal mesosphere, Geophys. Res. Lett., 42, 4639–4647, doi:10.1002/2015GL063724, 2015.

Shepherd, M., Shepherd, G., and Codrescu, M.: Perturbations of $O(^1D)$ VER, temperature, winds, atomic oxygen, and TEC at high southern latitudes, J. Geophys. Res., 124, 4773–4795, doi:10.1029/2019JA026480, 2019.

Shimazaki, T., and Laird, A. R.: A model calculation of the diurnal variation in minor neutral constituents in the mesosphere and lower thermosphere including transport effects, J. Geophys. Res., 75, 3221– 3235, doi:10.1029/JA075i016p03221, 1970.

https://doi.org/10.5194/angeo-2019-154
Preprint. Discussion started: 25 November 2019

Annales Geophysicae Discussions

Taniguchi, N., Hayashida, S., Takahashi, K., and Matsumi, Y.: Sensitivity studies of the recent new data on O(^{1}D) quantum yields in O_3 Hartley band photolysis in the stratosphere, Atmos. Chem. Phys., 3, 1293-1300, doi:10.5194/acp-3-1293-2003, 2003.

Zhu, Y., and Kaufmann, M.: Consistent nighttime atomic oxygen concentrations from O2 A-band, O(1S) green line, and OH airglow measurements as performed by SCIAMACHY, Geophys. Res. Lett., 46, 8536–8545, doi:10.1029/2019GL083550, 2019.

https://doi.org/10.5194/angeo-2019-154
Preprint. Discussion started: 25 November 2019

	Process	Rate coefficient
1	$H + O_3 \rightarrow O_2 + OH(v)$	$1.4\cdot10^{-10}\cdot\exp(-470/T)$ cm^3 s^{-1} OH(9) yield is $y_9 = 0.47$.
2	$OH(9) + O_2 \rightarrow$ products	$1.15\cdot10^{-11}\cdot\exp(195/T)$ cm^3 s^{-1}
3	$OH(9) + N_2 \rightarrow$ products	$5.03\cdot10^{-13}\cdot\exp(100/T)$ cm^3 s^{-1}
4	$OH(9) + O \rightarrow$ products	$6.2\cdot10^{-10}\cdot\exp(-135/T)$ cm^3 s^{-1} $O(^1D)$ yield is $y_1 = 5/6.2$
5	radiative decay of OH(9)	173 s^{-1}
6	$O(^1D) + O_2 \rightarrow O + O_2$	$3.3\cdot10^{-11}\cdot\exp(55/T)$ cm^3 s^{-1}
7	$O(^1D) + N_2 \rightarrow O + N_2$	$2.15\cdot10^{-11}\cdot\exp(110/T)$ cm^3 s^{-1}
8	radiative decay of $O(^1D)$	0.009 s^{-1}

Table 1. List of processes with corresponding rate coefficients from Kalogerakis et al. (2011), (2016), Sharma et al. (2015) and Burkholder et al. (2015).

https://doi.org/10.5194/angeo-2019-154
Preprint. Discussion started: 25 November 2019

Annales Geophysicae
Discussions
Open Access

Figures

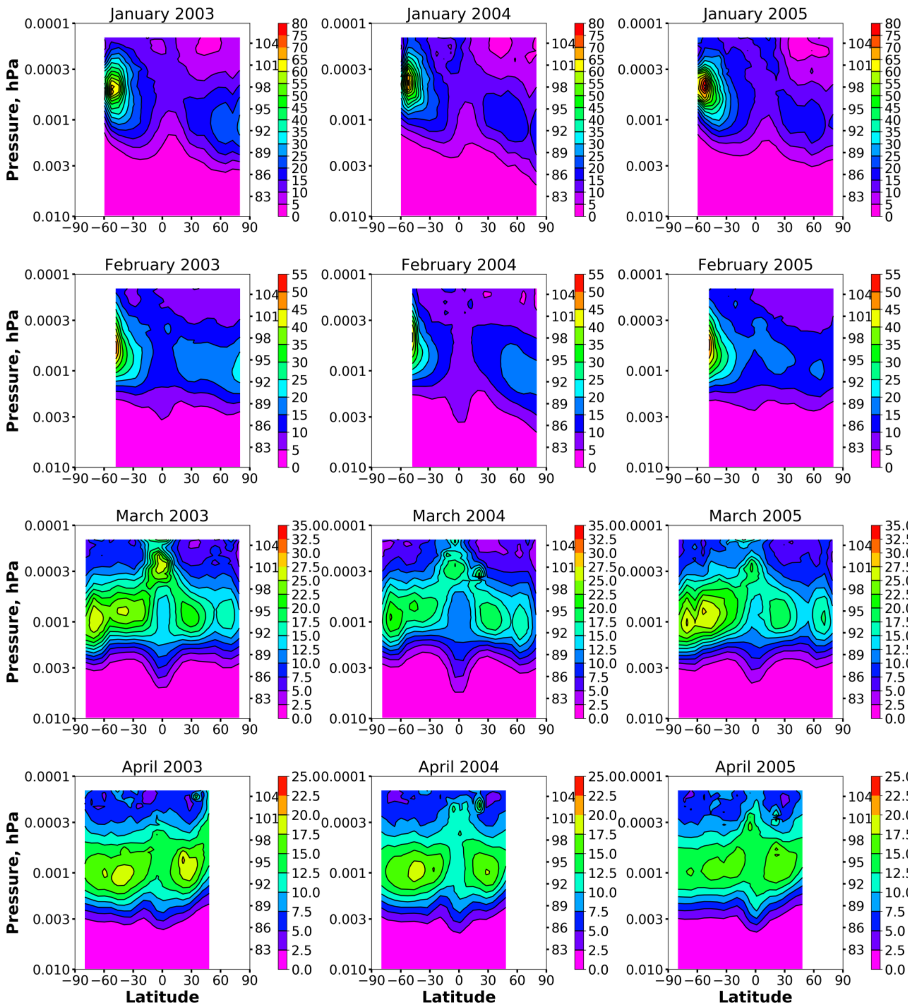

Figure 1. Monthly averaged O(^{1}D) concentration (in cm^{-3}) in different months of 2003-2005.

https://doi.org/10.5194/angeo-2019-154
Preprint. Discussion started: 25 November 2019

Annales Geophysicae Discussions
Open Access

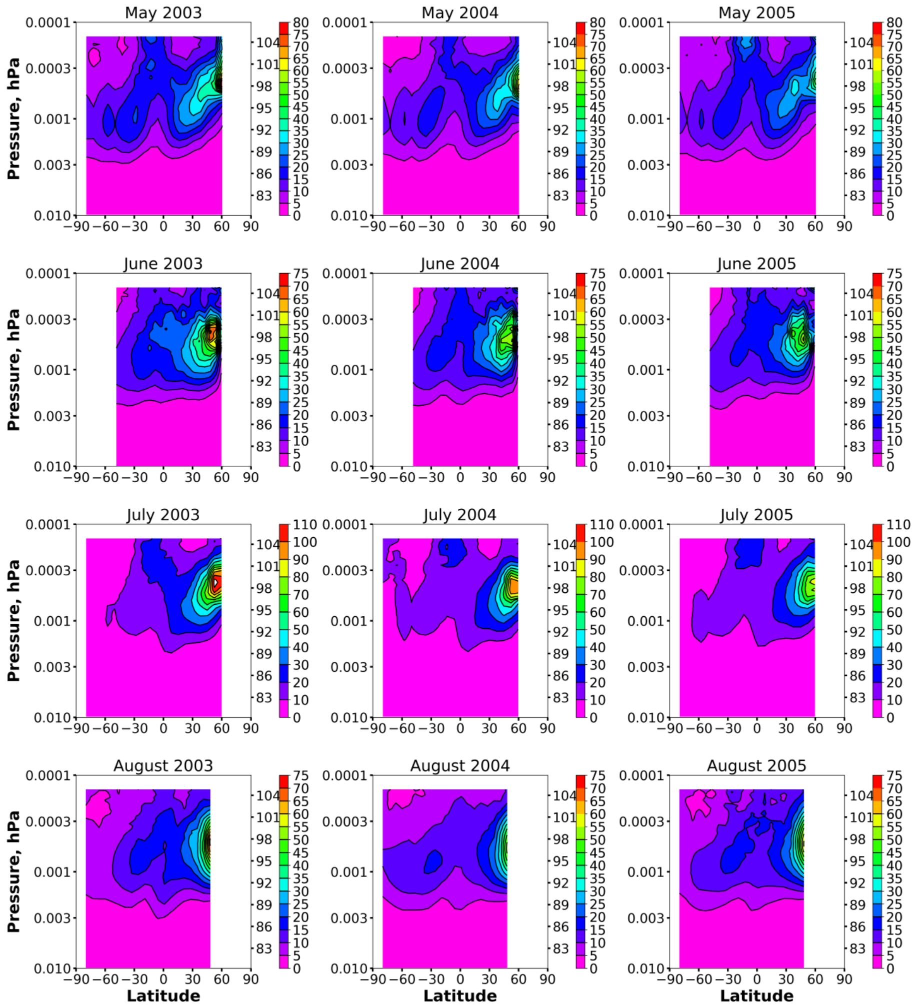

Figure 2. Monthly averaged $O(^1D)$ concentration (in cm^{-3}) in different months of 2003-2005.

https://doi.org/10.5194/angeo-2019-154
Preprint. Discussion started: 25 November 2019

Annales Geophysicae
Discussions
Open Access

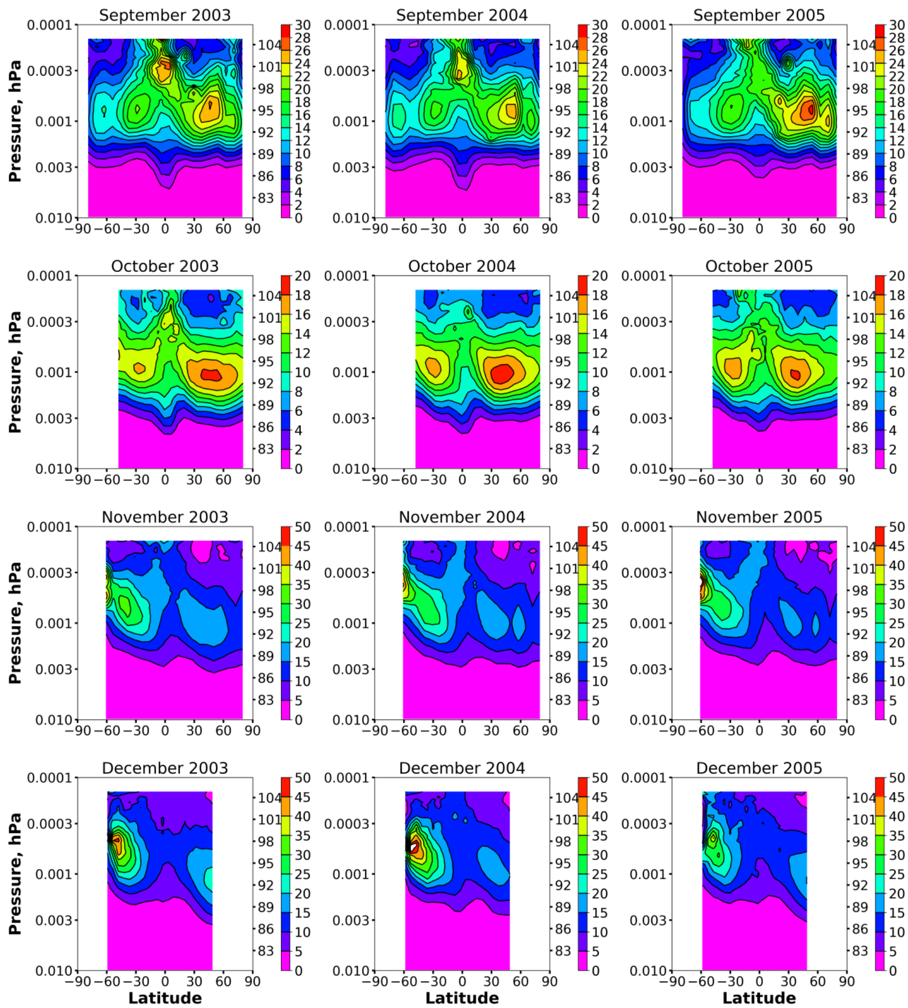

Figure 3. Monthly averaged O(^{1}D) concentration (in cm^{-3}) in different months of 2003-2005.

https://doi.org/10.5194/angeo-2019-154
Preprint. Discussion started: 25 November 2019

Annales Geophysicae Discussions Open Access EGU

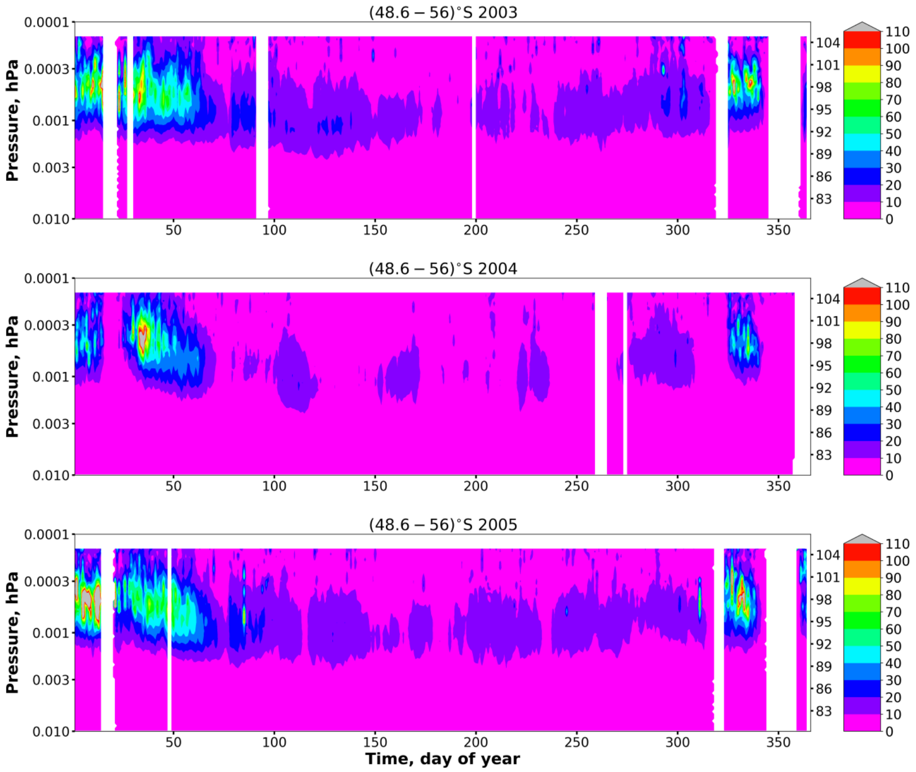

Figure 4. The nightly averaged $< O(^1D) >$ vertical distributions at (48-54)°S as a function of day of year. The values of $O(^1D)$ concentration greater than 110 cm^{-3} are grayed out.

https://doi.org/10.5194/angeo-2019-154
Preprint. Discussion started: 25 November 2019

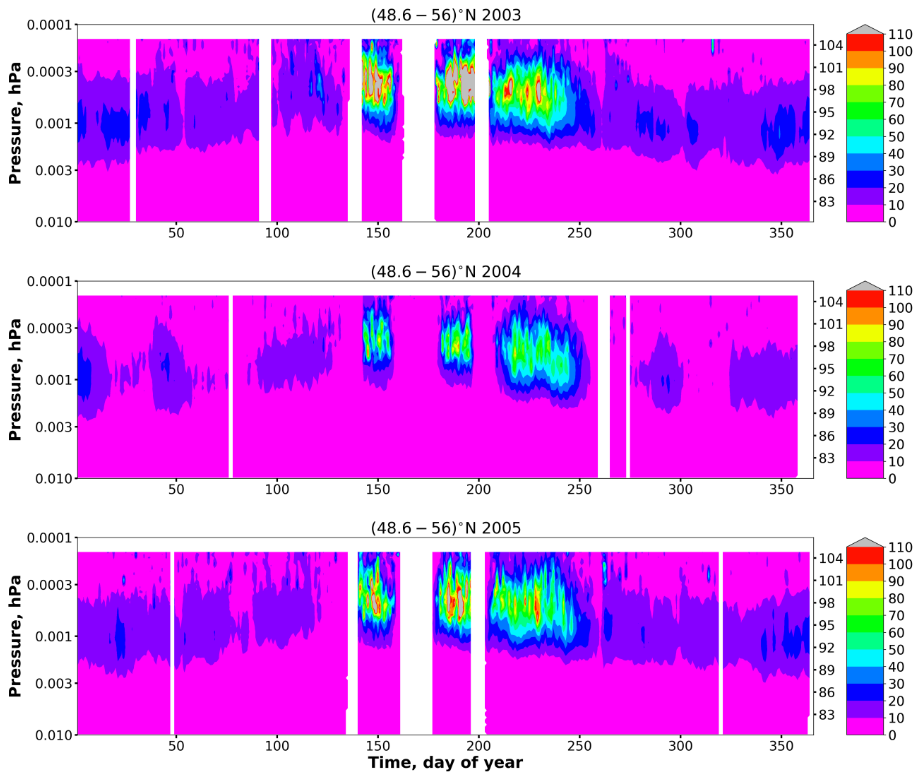

Figure 5. The nightly averaged $< O(^1D) >$ vertical distributions at (48-54)°N as a function of day of year. The values of $O(^1D)$ concentration greater than 110 cm^{-3} are grayed out.

https://doi.org/10.5194/angeo-2019-154
Preprint. Discussion started: 25 November 2019

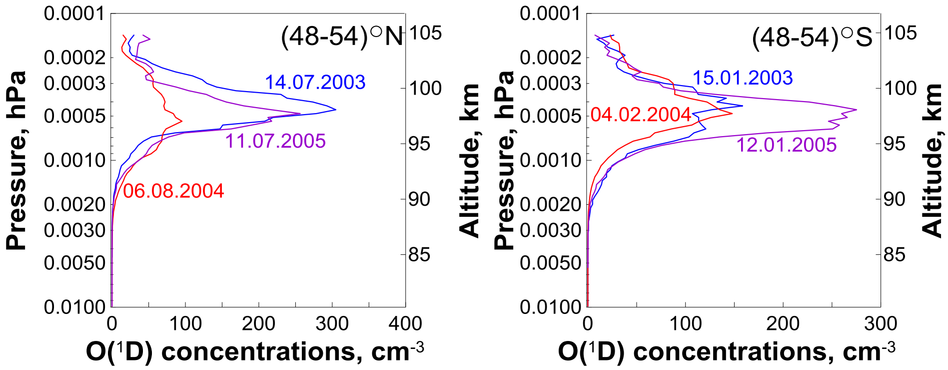

Figure 6. Examples of nightly averaged $< O(^1D) >$ profiles vertical distributions at (48-54)°N (left) and (48-54)°S (right).